AMERICAN SOCIETY FOR MICROBIOLOGY | Journal of Virology®

PATHOGENESIS AND IMMUNITY

An *In Vivo* Model of Echovirus-Induced Meningitis Defines the Differential Roles of Type I and Type III Interferon Signaling in Central Nervous System Infection

Alexandra I. Wells,[a] **Carolyn B. Coyne**[a,b]

[a]Department of Molecular Genetics and Microbiology, Duke University School of Medicine, Durham, North Carolina, USA
[b]Duke Human Vaccine Institute, Duke University School of Medicine, Durham, North Carolina, USA

ABSTRACT Echoviruses are among the most common worldwide causes of aseptic meningitis, which can cause long-term sequelae and death, particularly in neonates. However, the mechanisms by which these viruses induce meningeal inflammation are poorly understood, owing at least in part to the lack of *in vivo* models that recapitulate this aspect of echovirus pathogenesis. Here, we developed an *in vivo* neonatal mouse model that recapitulates key aspects of echovirus-induced meningitis. We show that expression of the human homologue of the primary echovirus receptor, the neonatal Fc receptor (FcRn), is not sufficient for infection of the brains of neonatal mice. However, ablation of type I, but not III, interferon (IFN) signaling in mice expressing human FcRn permitted high levels of echovirus replication in the brain, with corresponding clinical symptoms, including delayed motor skills and hind-limb weakness. Using this model, we defined the immunological response of the brain to echovirus infection and identified key cytokines, such as granulocyte colony-stimulating factor (G-CSF) and interleukin 6 (IL-6), that were induced by this infection. Lastly, we showed that echoviruses specifically replicate in the leptomeninges, where they induce profound inflammation and cell death. Together, this work establishes an *in vivo* model of aseptic meningitis associated with echovirus infections that delineates the differential roles of type I and type III IFNs in echovirus-associated neuronal disease and defines the specificity of echoviral infections within the meninges.

IMPORTANCE Echoviruses are among the most common worldwide causes of aseptic meningitis, which can cause long-term sequelae or even death. The mechanisms by which echoviruses infect the brain are poorly understood, largely owing to the lack of robust *in vivo* models that recapitulate this aspect of echovirus pathogenesis. Here, we establish a neonatal mouse model of echovirus-induced aseptic meningitis and show that expression of the human homologue of the FcRn, the primary receptor for echoviruses, and ablation of type I IFN signaling are required to recapitulate echovirus-induced meningitis and clinical disease. These findings provide key insights into the host factors that control echovirus-induced meningitis and a model that could be used to test anti-echovirus therapeutics.

KEYWORDS aseptic meningitis, echovirus, enterovirus, *in vivo*, neonatal Fc receptor

Enteroviruses are the main causes worldwide of aseptic meningitis, which is characterized by meningeal inflammation not associated with any identifiable bacterial species in cerebrospinal fluid (CSF). Approximately 90% of aseptic meningitis cases in infants (1) and 50% in older children and adults (2) are caused by enteroviruses, with the group B enterovirus members coxsackievirus B (CVB) and echoviruses being among the most common (3, 4). Infants and young children are particularly vulnerable to echovirus-associated neuronal complications, which can cause long-term sequelae,

Editor Colin R. Parrish, Cornell University

Address correspondence to Carolyn B. Coyne, carolyn.coyne@duke.edu.
The authors declare no conflict of interest.

Received 21 February 2022
Accepted 20 April 2022
Published 14 June 2022

including seizure disorders (5, 6), and are associated with high rates of death, which occurs in as many as one-third of cases (7, 8). Several echoviruses, including echovirus 5 (E5), E9, E11, and E30, have been associated with outbreaks, including cases of aseptic meningitis (4, 9). Despite the clear association between echoviruses and aseptic meningitis, the mechanisms by which these viruses induce meningeal inflammation are poorly understood, owing at least in part to the lack of *in vivo* models that recapitulate this aspect of echovirus pathogenesis.

Echoviruses are the largest subgroup of the *Enterovirus* genus and consist of approximately 30 serotypes. Recent studies have shown that the neonatal Fc receptor (FcRn) is the primary entry receptor for echoviruses (10, 11). Outside infection, FcRn transports and regulates the circulating half-life of immunoglobulin G (IgG) and is enriched in the endothelium of the central nervous system (CNS), including the blood-brain barrier (BBB), where it mediates the efflux of IgG from the brain (12–16). Although several studies have investigated the possible mechanistic basis for CVB-associated neuronal dysfunction *in vitro* and *in vivo* (17–19), much less is known about echovirus-associated CNS complications. Intracerebral inoculation of newborn mice expressing VLA-2, a reported receptor for E1, yields paralysis and motor defects (20). Other work suggests that type I interferons (IFNs) play a role in E11 CNS disease following intracranial inoculation (21). However, because both of those studies used intracranial inoculation, the host factors that permit access to the CNS are unclear. We previously generated an *in vivo* mouse model of E11 pathogenesis using adult and neonatal mice and showed that expression of the human homologue of FcRn in mice lacking type I IFN signaling were susceptible to echovirus infection following intraperitoneal (i.p.) inoculation, including infection of the brain (22). However, the consequences of echovirus infection, including the induction of cytokines and cell death in the brains of the mice, and identification of the region(s) of the brain targeted by infection were not explored.

The meninges surround the brain and are composed of three distinct membranous layers, namely, the dura mater, arachnoid mater, and pia mater. A hallmark of aseptic meningitis involves inflammation of the meninges, resulting in immune cell infiltration and swelling. In human cases of confirmed echovirus aseptic meningitis, infection is associated with a robust inflammatory response, as indicated by the presence of high levels of proinflammatory mediators in CSF, including interleukin 6 (IL-6) and monocyte chemoattractant protein 1 (MCP-1) (23–25). Higher levels of type I IFNs are also present in CSF isolated from enterovirus-associated meningitis than in that from bacterial meningitis (26), suggesting that these IFNs play a prominent role in aseptic meningitis. Type I IFNs, which include IFN-αs and IFN-β, provide key antiviral defenses from many neurotropic viruses, including flaviviruses, alphaviruses, and herpesviruses (27). In some cases, type III IFNs (IFN-λs) also defend from CNS viral infections (28, 29), and they have been proposed to function by alterations in BBB permeability (28). While the type I IFN receptor (IFNAR) is present on all nucleated cells, the type III IFN receptor (IFNLR) is restricted in expression but is expressed on cells within the BBB (reviewed in reference 30). Thus, although previous studies suggested a potential role for both type I and type III IFNs during neurotropic viral infection of the CNS, whether type I and type III IFNs play different roles in echovirus infections of the CNS is unknown.

Here, we developed an *in vivo* model of echovirus-induced aseptic meningitis in neonatal mice that recapitulates many of the disease manifestations observed in humans. We show that expression of human FcRn alone is not sufficient to mediate echovirus infection of the brains of 7-day-old neonatal mice. In addition, the brains of mice deficient in either type I or type III IFN signaling alone were not permissive to echovirus infection. In contrast, we found that humanized FcRn mice deficient in IFNAR, but not IFNLR, exhibited high levels of echovirus replication in the brain with corresponding clinical symptoms, including hind-limb weakness and paralysis. Using this model, we defined the immune response in the brains of echovirus-infected mice, which included the induction of high levels of IL-6, C-X-C motif chemokine ligand 10 (CXCL10), and granulocyte colony-stimulating factor 3 (G-CSF-3). Lastly, we show that

echoviruses replicate in the leptomeninges and induce inflammation and cytotoxicity in these membranes, including activation of apoptotic cell death. Together, this work establishes an *in vivo* model of aseptic meningitis associated with echovirus infections and defines the specificity of echoviral infections in the meninges.

RESULTS

Ablation of type I IFN signaling and human FcRn expression are required for echovirus infection of the brain. Previously, we developed a mouse model of echovirus pathogenesis using E11 through i.p. inoculation of mice expressing the human homologue of FcRn (hFcRn^{Tg32}) and also ablated in type I IFN signaling by deletion of IFNAR (hFcRn^{Tg32}-IFNAR$^{-/-}$) (22). hFcRn^{Tg32} mice are deficient in expression of mouse FcRn and express hFcRn under the control of the native human promoter (31). To determine whether type III IFNs also play a role in echovirus infections at secondary sites of infection, including the brain, we used hFcRn^{Tg32} mice deficient in expression of IFNLR, the receptor for type III IFNs (hFcRn^{Tg32}-IFNLR$^{-/-}$) (32). These studies included six genotypes of mice, including the hFcRn-expressing mice described above (hFcRn^{Tg32}, hFcRn^{Tg32}-IFNAR$^{-/-}$, and hFcRn^{Tg32}-IFNLR$^{-/-}$) and animals expressing murine FcRn that were immunocompetent (C57/BL6, i.e., wild type [WT]) or deficient in type I or type III IFN signaling (IFNAR$^{-/-}$ or IFNLR$^{-/-}$, respectively) (Fig. 1A). To specifically focus on the role of FcRn in echovirus pathogenesis, we used E5, which, unlike other echoviruses such as E11 and E30, does not bind additional attachment receptors such as complement decay-accelerating factor (DAF)/CD55 (10, 33). Neonatal (7-day-old) mice were inoculated with 10^4 PFU of E5 by the i.p. route and monitored for 3 days postinoculation (dpi). Infection resulted in clear motor function delays and death, with death in 100% of hFcRn^{Tg32}-IFNAR$^{-/-}$ animals by 2 dpi (Fig. 1B). In contrast, there were no clinical symptoms of illness in any other genotype, and all animals survived until 3 dpi (Fig. 1B). There were no significant differences in mortality rates between male and female hFcRn^{Tg32}-IFNAR$^{-/-}$ mice (Fig. 1C). We next determined the levels of circulating virus in the blood and brains of these animals. We detected high levels of E5 in the blood (6 of 6 mice) and brains (12 of 12 mice) of hFcRn^{Tg32}-IFNAR$^{-/-}$ mice but no detectable virus in any other genotype (Fig. 1D and E). There were no significant differences in E5 titers in the brains of male or female hFcRn^{Tg32}-IFNAR$^{-/-}$ mice (Fig. 1F).

Consistent with our previous findings with E11 (22), we found that there was robust replication in the livers and pancreases of E5-infected hFcRn^{Tg32}-IFNAR$^{-/-}$ mice (12 of 12 mice) (Fig. 1G and H). However, in contrast to the brain, we found that hFcRn^{Tg32}-IFNLR$^{-/-}$ animals also contained virus in the liver (4 of 8 mice) and pancreas (8 of 8 mice) (Fig. 1G and H). We also detected low to midrange levels of E5 in the pancreases of immunocompetent hFcRn^{Tg32} mice (5 of 5 mice) and to a much lesser extent in liver (1 of 5 mice) (Fig. 1G and H). There was no detectable virus in any animals expressing the murine homologue of FcRn (Fig. 1G and H), consistent with our previous work (22). Collectively, these data show that echovirus infections in the brain require expression of hFcRn and that the primary barrier to infection is type I IFN-mediated signaling.

Echovirus infections cause paralysis and motor defects in infected mice. Because we observed high mortality rates in mice infected with 10^4 PFU E5 by the i.p. route, we investigated the neurotropism and neurovirulence of E5 in mice infected with a lower inoculum (10^3 PFU) of E5 by the i.p. route. With this smaller inoculum, we observed death in approximately 50% of hFcRn^{Tg32}-IFNAR$^{-/-}$ animals by 1.5 to 2 dpi, compared to no deaths among hFcRn^{Tg32}-IFNLR$^{-/-}$ animals (Fig. 2A). There were no differences in mortality rates between male and female hFcRn^{Tg32}-IFNAR$^{-/-}$ mice (Fig. 2B). Infected animals were monitored for signs of illness (e.g., delayed movements, paralysis, discoloration, lack of nursing, lack of parental care, and death) throughout the duration of infection. There were no signs of clinical illness in echovirus-infected hFcRn^{Tg32}-IFNLR$^{-/-}$ animals at 1 or 2 dpi (Fig. 2C). There were also no obvious clinical symptoms in hFcRn^{Tg32}-IFNAR$^{-/-}$ animals at 1 dpi. By 1.5 to 2 dpi, however, there were clear defects in motor skills and various degrees of paralysis in infected hFcRn^{Tg32}-IFNAR$^{-/-}$ animals. There were a range of defects, i.e., mild loss of motor function in

A

Strain	Expression			
	mFcRn	hFcRn	IFNAR	IFNLR
C57BL/6J	+	-	+	+
hFcRn^{Tg32}	-	+	+	+
IFNAR$^{-/-}$	+	-	-	+
hFcRn^{Tg32}-IFNAR$^{-/-}$	-	+	-	+
IFNLR$^{-/-}$	+	-	+	-
hFcRn^{Tg32}-IFNLR$^{-/-}$	-	+	+	-

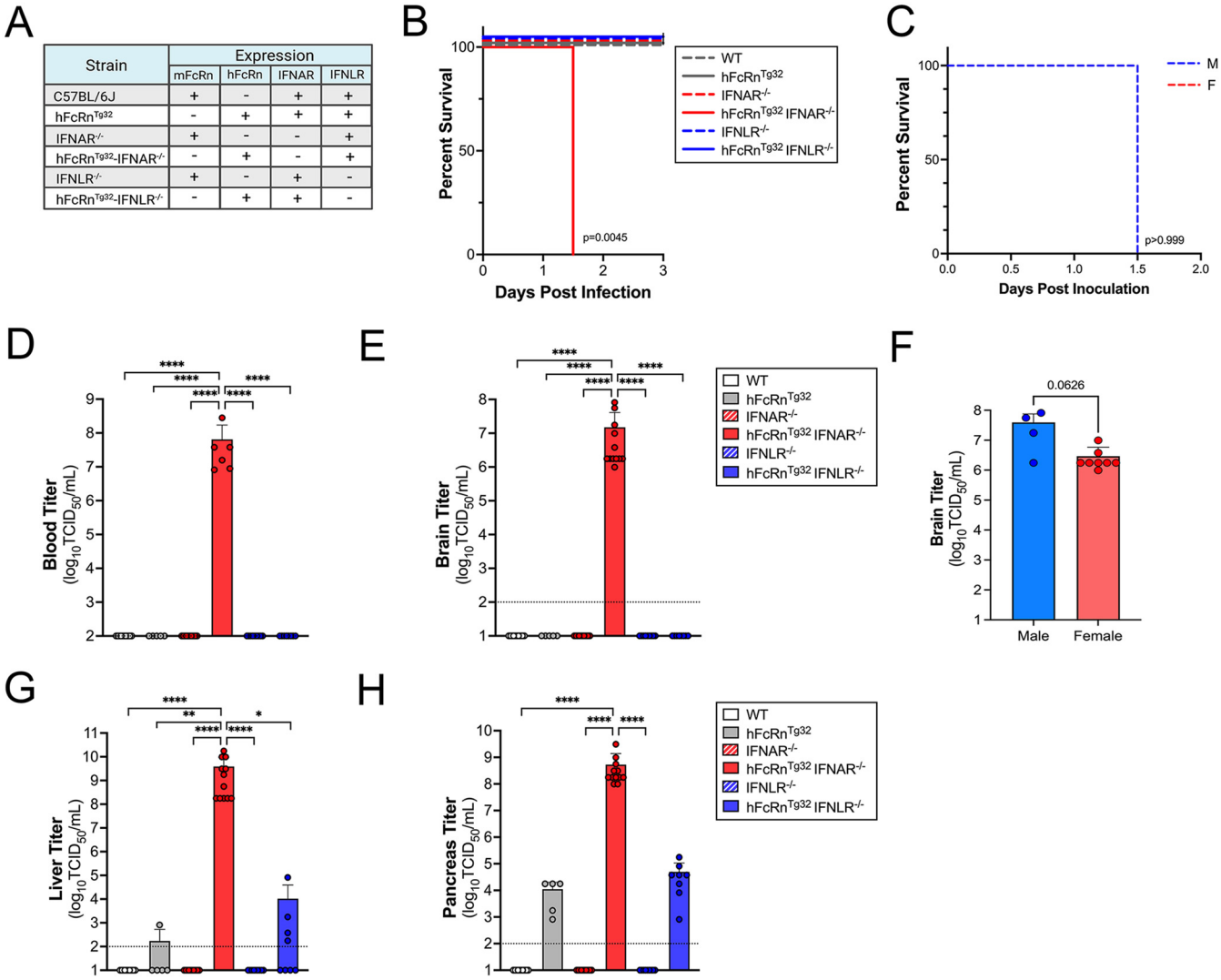

FIG 1 Ablation of type I IFN signaling and human FcRn expression are required for echovirus infection in the brain. (A) Table of the six genotypes used in this study. Shown is the expression of mouse or human FcRn, IFNAR, and IFNLR among these genotypes. (B) Survival of the indicated genotype of mice inoculated with 10^4 PFU of E5 by the i.p. route and monitored every 12 h for 3 dpi. The number of pups for each genotype was as follows: WT, $n = 17$; hFcRn^{Tg32}, $n = 6$; IFNAR$^{-/-}$, $n = 17$; hFcRn^{Tg32}-IFNAR$^{-/-}$, $n = 12$; IFNLR$^{-/-}$, $n = 14$; hFcRn^{Tg32}-IFNLR$^{-/-}$, $n = 8$. The log rank test was used to analyze the statistical difference in the survival rates. Surviving genotypes were separated for visualization. (C) Survival of hFcRn^{Tg32}-IFNAR$^{-/-}$ mice inoculated with 10^4 PFU of E5 by the i.p. route and monitored for 3 dpi. Animals are divided by sex (M, male; F, female) to represent any potential sex differences in mortality rates. The log rank test was used to analyze the statistical difference in the survival rates, with the *P* value shown. (D and E). At 3 dpi, animals were sacrificed and viral titers in blood (D) and brain (E) were determined by $TCID_{50}$ assays. Titers are shown as $log_{10}TCID_{50}$ per milliliter, with the limit of detection indicated by a dotted line. Data are shown as mean ± standard deviation, with individual animals shown as data points. (F) Brain titers for hFcRn^{Tg32}-IFNAR$^{-/-}$ animals divided by sex. Data are shown with significance determined with a Mann-Whitney U test, with the *P* values indicated. (G and H) Titers for the indicated genotypes of mice inoculated with 10^4 PFU of E5 by the i.p. route. At 3 dpi, animals were sacrificed, and viral titers in liver (G) and pancreas (H) were determined by $TCID_{50}$ assays. Titers are shown as $log_{10}TCID_{50}$ per milliliter, with the limit of detection indicated by a dotted line. Data are shown as mean ± standard deviation, with individual animals shown as data points. Data are shown with significance determined with a Kruskal-Wallis test with a Dunn's test for multiple comparisons. *, $P < 0.05$; **, $P < 0.005$; ****, $P < 0.0001$.

one or more limb, characterized by difficulty walking, hemiplegia that obstructed mobility, or hind-limb paralysis (Fig. 2C). To correlate clinical symptoms with infection, we titrated virus from the brains of infected animals at 1 and 2 dpi, which revealed similar titers in brain on the two days and higher titers in blood at 2 dpi in hFcRn^{Tg32}-IFNAR$^{-/-}$ animals (Fig. 2D). There were no differences in titers between male and female mice (Fig. 2E). Additionally, like the lack of clinical disease and low morality rates, no virus was detected in the blood or brains of hFcRn^{Tg32}-IFNLR$^{-/-}$ animals (Fig. 2D). These data show that echoviruses induce clinical symptoms of neurological disease, which occurs in an hFcRn-dependent manner and requires ablation of type I IFN signaling.

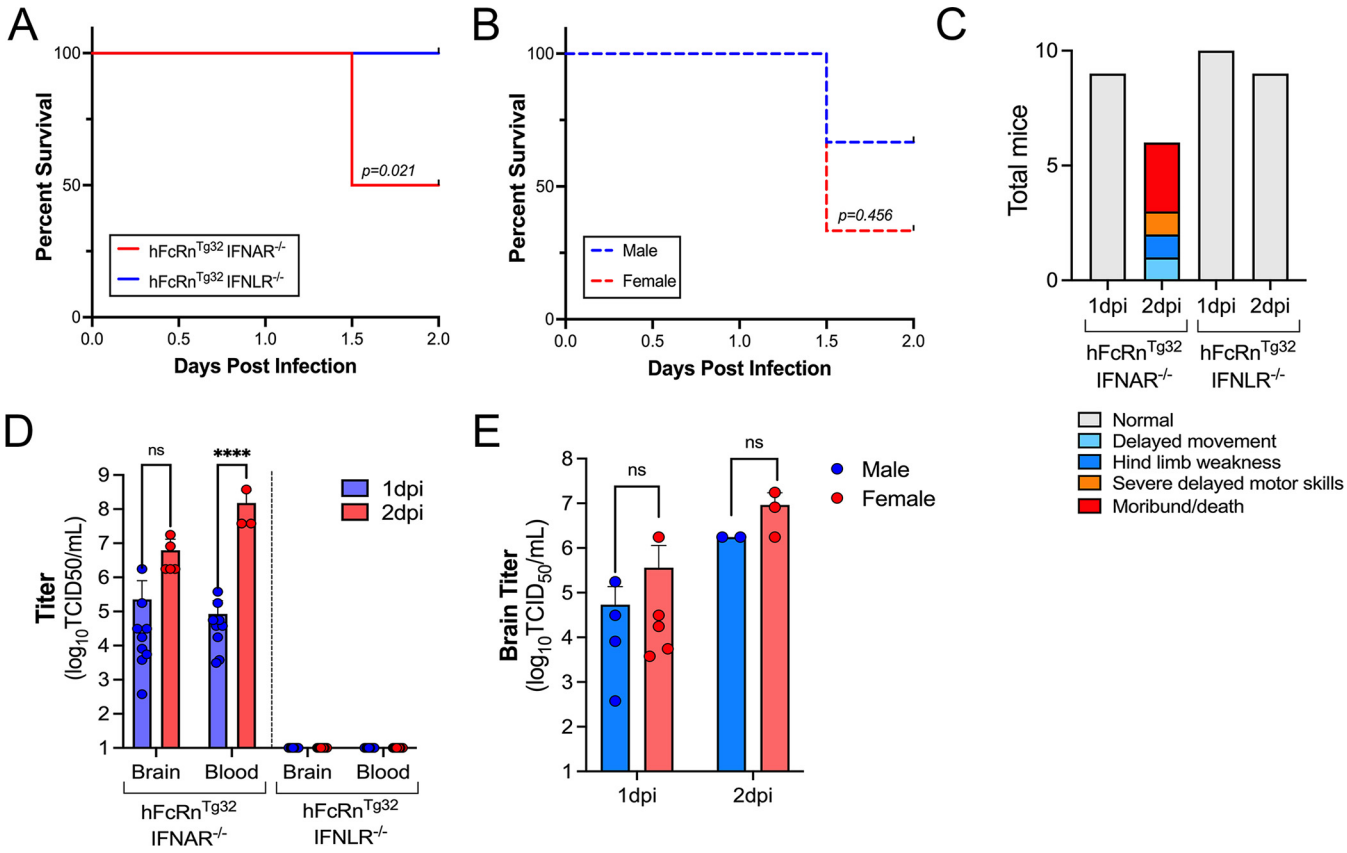

FIG 2 Echovirus infections cause paralysis and motor defects in infected mice. hFcRn^{Tg32}-IFNAR$^{-/-}$ and hFcRn^{Tg32}-IFNLR$^{-/-}$ mice were inoculated with 10^3 PFU of E5 by the i.p. route and monitored for signs of disease. (A) Survival of the indicated genotype of mice inoculated with 10^3 PFU of E5 by the i.p. route and monitored every 12 h for 2 dpi. The number of pups for each genotype was as follows: hFcRn^{Tg32}-IFNAR$^{-/-}$, $n = 14$; hFcRn^{Tg32}-IFNLR$^{-/-}$, $n = 19$. The log rank test was used to analyze the statistical difference in the survival rates. (B) Survival of hFcRn^{Tg32}-IFNAR$^{-/-}$ mice inoculated with 10^3 PFU of E5 by the i.p. route and monitored for 2 dpi. Animals are divided by sex to represent any potential sex differences in mortality rates. The log rank test was used to analyze the statistical difference in the survival rates, with the *P* value shown. (C) Clinical symptoms observed for hFcRn^{Tg32}-IFNAR$^{-/-}$ or hFcRn^{Tg32}-IFNLR$^{-/-}$ pups at either 1 or 2 dpi. Animals were monitored for delayed movement when moved outside the litter, hind-limb weakness (based on the ability to use the limbs while walking and potential dragging of limbs), severe delayed motor skills (if animals had trouble walking back to their littermates), or moribundity/death. (D) At 1 or 2 dpi, animals were sacrificed and viral titers in blood and brain were determined by $TCID_{50}$ assays. Titers are shown as $\log_{10}TCID_{50}$ per milliliter, with the limit of detection indicated by a dotted line. Data are shown as mean ± standard deviation, with individual animals shown as data points. Data are shown with significance determined with a two-way ANOVA with Šídák's multiple-comparison tests. ****, $P < 0.0001$; ns, not significant. (E) Brain titers from hFcRn^{Tg32}-IFNAR$^{-/-}$ animals divided by sex at either 1 or 2 dpi. Data are shown with significance determined with a Mann-Whitney U test.

Immunological signature of echovirus-infected brains. To define the immunological signature of echovirus-infected brains, we harvested the brains of E5-infected mice expressing hFcRn (hFcRn^{Tg32}, hFcRn^{Tg32}-IFNAR$^{-/-}$, or hFcRn^{Tg32}-IFNLR$^{-/-}$) at 3 dpi and performed multianalyte Luminex-based profiling of 27 cytokines and chemokines in brain tissue homogenates. We found that echovirus infection induced high levels of cytokines in brain tissue of infected hFcRn^{Tg32}-IFNAR$^{-/-}$ mice at 3 dpi, including high levels of G-CSF-3, which was the most abundant cytokine detected (~750-fold over uninfected mice) (Fig. 3A and C). Other highly induced cytokines included IL-6 (25-fold over uninfected mice), CXCL10 (17-fold over uninfected mice), MCP-1 (16-fold over uninfected mice), and keratinocyte-derived chemokine (KC) (12-fold over uninfected mice) (Fig. 3A, D, E, and F). There was no significant induction of any cytokines in infected hFcRn^{Tg32} or hFcRn^{Tg32}-IFNLR$^{-/-}$ animals at 3 dpi (Fig. 3A). We did not detect the type I IFNs IFN-α2 and IFN-β or the type III IFN IFN-λ1 in the brains of any mice (Fig. 3A).

We next assessed the kinetics of cytokine induction in echovirus-infected brains isolated from infected hFcRn^{Tg32}-IFNAR$^{-/-}$ and hFcRn^{Tg32}-IFNLR$^{-/-}$ animals at 1 and 2 dpi. Consistent with the overall low levels of virus in the brains of mice at 1 dpi, we observed

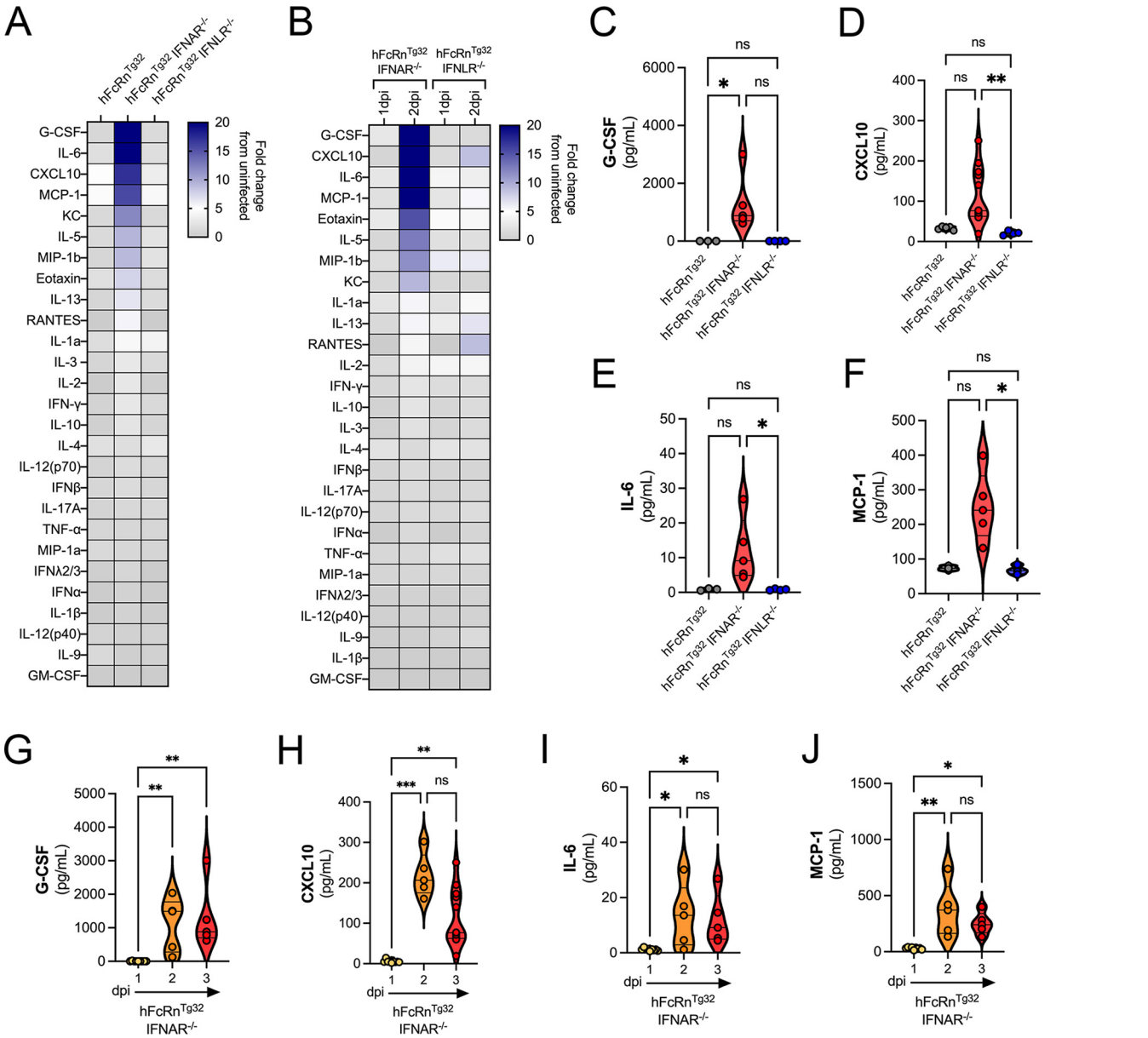

FIG 3 Immunological signature of echovirus-infected brains. Pups were i.p. inoculated and sacrificed at either 1, 2, or 3 dpi. Cytokine expression in brain tissue homogenates was analyzed by multiplex Luminex assays. (A) Heatmap demonstrating the induction (shown as fold change from uninfected controls) in E5-infected mice of the indicated genotype sacrificed at 3 dpi. Blue denotes significantly increased cytokines, in comparison to untreated controls. Gray or white denotes little to no change (scale at top right). (B) Heatmap demonstrating the induction (shown as fold change from hFcRn^{Tg32} pups) in E5-infected mice of the indicated genotype sacrificed at 1 or 2 dpi, as indicated. Blue denotes significantly increased cytokines, in comparison to untreated controls. Gray or white denotes little to no change (scale at top right). (C to F) Top four cytokines induced from animals sacrificed at 3 dpi from panel A, including G-CSF (C), CXCL10 (D), IL-6 (E), and MCP-1 (F). (G to J) Top four cytokines induced in hFcRn^{Tg32}-IFNAR$^{-/-}$ animals over the course of the infection time. Shown are G-CSF (G), CXCL10 (H), IL-6 (I), and MCP-1 (J). Data are shown as mean ± standard deviation, with individual animals shown as data points. Data are shown with significance determined with a Kruskal-Wallis test with a Dunn's test for multiple comparisons. *, $P < 0.05$; **, $P < 0.005$; ***, $P < 0.0005$; ns, not significant.

very little cytokine induction in hFcRn^{Tg32}-IFNAR$^{-/-}$ animals at this time (Fig. 3B). By 2 dpi, however, there were high levels of cytokines similar to those observed at 3 dpi, including G-CSF (647-fold over uninfected mice), CXCL10 (33-fold over uninfected mice), IL-6 (28-fold over uninfected mice), and MCP-1 (23-fold over uninfected mice) (Fig. 3B and G to J). No cytokines were significantly induced in infected hFcRn^{Tg32}-IFNLR$^{-/-}$ animals at either time point, although in some cases outlier samples skewed the average fold induction to >5-fold (Fig. 3B). These data show that echovirus infection of brain

tissue results in an immunological response characterized by the induction of select proinflammatory cytokines and chemokines.

Echoviruses replicate in the leptomeninges to induce meningeal inflammation. Very little is known regarding the cellular or structural targets of echovirus infections in the brain, including the meninges, which is composed of three membranous layers. To define the site(s) of echovirus replication in the brain, we infected hFcRn^{Tg32}, hFcRn^{Tg32}-IFNAR$^{-/-}$, and hFcRn^{Tg32}-IFNLR$^{-/-}$ mice with 10^4 PFU E5 for 2 to 3d to maximize infection. At that time, whole brains were removed, sectioned, and processed for hybridization chain reaction (HCR) using E5-specific probes. HCR allows for fluorescent quantitative RNA detection with enhanced sensitivity, compared with conventional hybridization approaches, given signal amplification resulting from the self-assembly of secondary detection hairpins into amplification polymers (34, 35). Whole-brain confocal microscopy-based tile scanning of ~36 mm^2 was then performed to define the region(s) infected by E5. We observed high levels of E5 viral RNA (vRNA) in infected hFcRn^{Tg32}-IFNAR$^{-/-}$ brain tissue at 3 dpi but none in hFcRn^{Tg32} or hFcRn^{Tg32}-IFNLR$^{-/-}$ brains; the vRNA was localized to a distinct region surrounding the brain (Fig. 4A). This region was specific for the leptomeninges, which includes the two inner layers of the meninges (Fig. 4B and C). In addition, there were concentrated regions of high levels of E5 vRNA surrounding blood vessels localized throughout the meninges (Fig. 4D). Although the choroid plexus has been reported to express high levels of FcRn (16), we did not detect any infection in this region (Fig. 4E). To determine the timing of E5 vRNA in the meninges, we performed HCR in whole brains isolated from hFcRn^{Tg32}-IFNAR$^{-/-}$ mice infected with E5 at 1 to 3 dpi. At 1 dpi, we found that the levels of E5 vRNA were undetectable, as in uninfected controls; by 2 dpi, however, there were clear areas of E5 infection, which significantly increased by 3 dpi (Fig. 4F and G).

To define the localization of FcRn within the brains of hFcRn^{Tg32} mice and to correlate this expression with E5 infection, we performed immunohistochemistry (IHC) for hFcRn in hFcRn^{Tg32}-IFNAR$^{-/-}$ mice. We found that hFcRn was enriched in the leptomeninges of infected animals, where it was concentrated to regions associated with high levels of vRNA (Fig. 5A).

Next, we assessed the impacts of E5 infection on the integrity of the meninges. We noted instances of acute meningitis and inflammatory tissue damage in hFcRn^{Tg32}-IFNAR$^{-/-}$ mice infected with E5 for 3 dpi, which included areas of immune cell infiltration (Fig. 5B). Areas of inflammation correlated with high levels of E5 replication, as indicated by aligning HCR and hematoxylin and eosin (H&E)-stained images (Fig. 5C). Lastly, to determine whether E5 infection induced direct cell death or damage to the meninges, we performed IHC for cleaved caspase 3, which revealed discrete areas of apoptosis as early as 2 dpi, with more significant levels at 3 dpi (Fig. 5D). Together, these data show that echovirus infection of the meninges induces pronounced tissue damage and inflammation.

DISCUSSION

Echovirus infections are common causes of neonatal meningitis, which can be fatal. However, how these viruses infect the brain and their regional tropism within the brain remain unknown. Here, we developed an *in vivo* model of echovirus-induced meningitis and used this model to define the regional targets and host immune pathways associated with echovirus infection within the brain. We show that expression of the human homologue of FcRn is necessary, but not sufficient, for echovirus infection of the brain. In addition, we show that type I IFNs, but not type III IFNs, provide a barrier to echovirus infection of the meninges and that ablation of this pathway sensitizes the brain to infection, which induces a robust immune response. Lastly, we define the specificity of echovirus replication in the brain and show that high levels of replication in the leptomeninges induce inflammation and cell death. These studies thus provide key insights into the events associated with echovirus-induced meningitis and an *in vivo* model that could be used to test echovirus therapeutics targeting echovirus-induced neuronal disease.

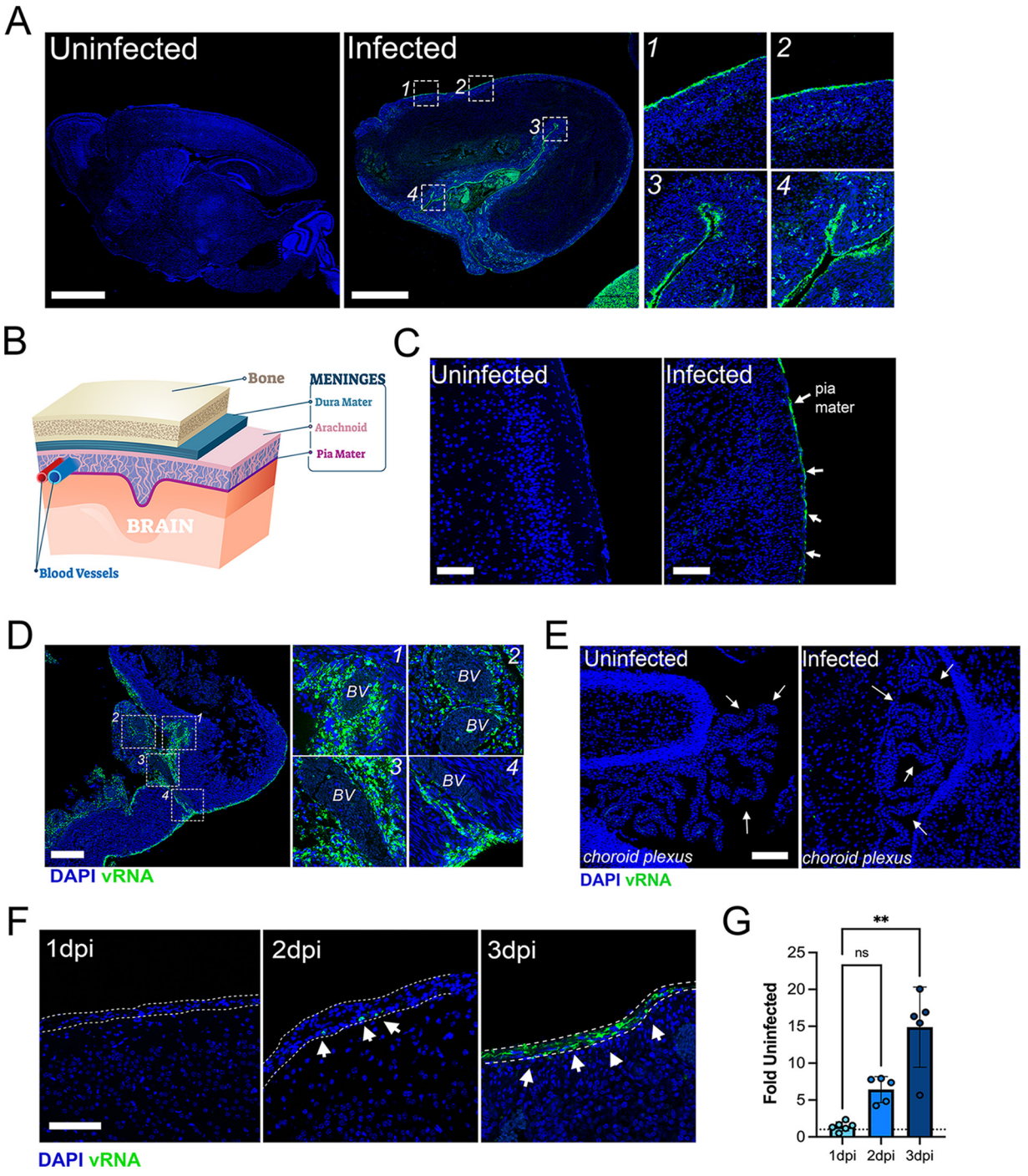

FIG 4 Echovirus replication in the leptomeninges. (A) Tile scan of the brains from an uninfected animal (left) and E5-infected hFcRn^{Tg32}-IFNAR$^{-/-}$ animal at 3 dpi (middle) using HCR for vRNA (in green) and DAPI (in blue). Numbered white boxes show zoomed areas to the right. (B) Schematic representation of the different layers of the meninges surrounding the brain. The dura mater is in teal, with the leptomeninges (arachnoid layer and pia mater) in shades of pink. (C) HCR for vRNA (in green) and DAPI (in blue) of the brain from an uninfected or E5-infected hFcRn^{Tg32}-IFNAR$^{-/-}$ animal at 3 dpi. White arrows denote areas of vRNA. (D) Tile scan of HCR for E5 vRNA from the brain of an infected hFcRn^{Tg32}-IFNAR$^{-/-}$ animal at 3 dpi with areas of infection surrounding blood vessels (BV). DAPI-stained nuclei are in blue, and vRNA is in green. White boxes indicate zoomed images at the right, with numbers in the top right corner denoting the corresponding zoomed image. (E) Choroid plexus region within the brain from uninfected (left) and E5-inoculated (right) hFcRn^{Tg32}-IFNAR$^{-/-}$ animals at 3 dpi using HCR with vRNA (in green) and DAPI (in blue). White arrows show the choroid plexus. (F) HCR for vRNA (in green) and DAPI (in blue) in the brains from infected hFcRn^{Tg32}-IFNAR$^{-/-}$ animals at 1, 2, or 3 dpi, as indicated at the top left. Dashed lines highlight the leptomeninges, and arrows denote infected cells. (G) Image analysis of the extent of vRNA signal in the brains of hFcRn^{Tg32}-IFNAR$^{-/-}$ animals at 1 to 3 dpi, shown as a fold change from uninfected controls. Symbols represent unique regions used in quantification. Data are shown with significance determined with a Kruskal-Wallis test with a Dunn's test for multiple comparisons. **, $P < 0.01$; ns, not significant. Scale bars are 1 mm (A), 100 μm (C), 1 mm (D), 100μm (E), and 50 μm (F).

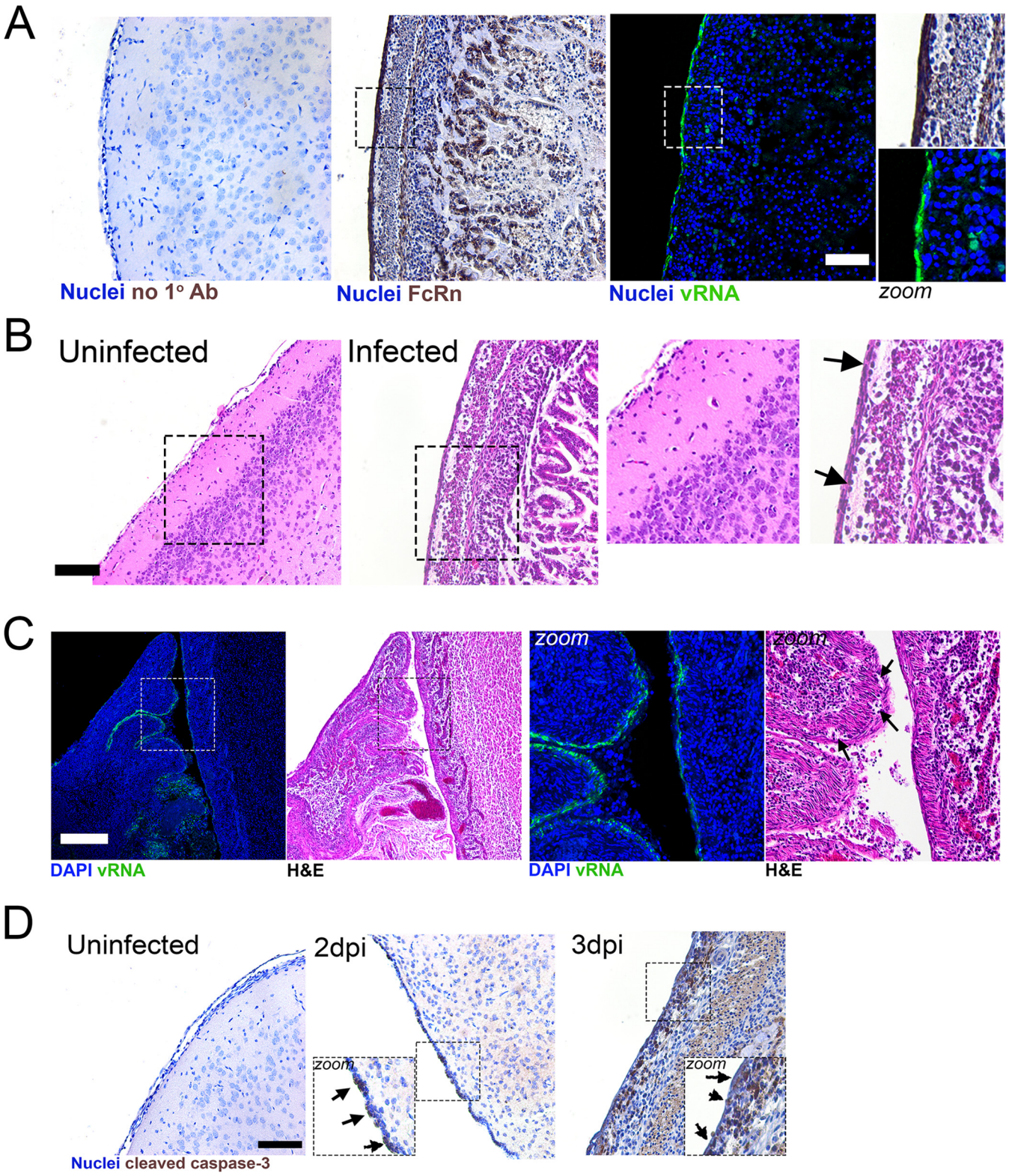

FIG 5 Echovirus replication in the meninges induces inflammation and cell death. (A) IHC for hFcRn and HCR for vRNA in the brain of a hFcRn^{Tg32}-IFNAR$^{-/-}$ animal infected with E5 for 3 days. Left, no-primary-antibody control in an uninfected control animal; middle, hFcRn IHC; right, HCR for vRNA (in green) and DAPI (in blue) from the same E5-infected hFcRn^{Tg32}-IFNAR$^{-/-}$ animal. Boxes indicate regions that are zoomed at the right. (B) H&E staining of representative brain sections from an uninfected or E5-infected hFcRn^{Tg32}-IFNAR$^{-/-}$ animal. Black boxes show areas of zoomed images at the right. Arrows denote regions of inflammation within the meninges. (C) HCR for E5 vRNA or H&E staining of the cerebellum within the brain of a hFcRn^{Tg32}-IFNAR$^{-/-}$ animal at 3 dpi. HCR shows vRNA (in green) and DAPI (in blue). Boxes denote areas of zoomed images at the right. Arrows denote regions of inflammation within the meninges. (D) IHC for cleaved caspase 3 in uninfected hFcRn^{Tg32}-IFNAR$^{-/-}$ animals or hFcRn^{Tg32}-IFNAR$^{-/-}$ animals infected with E5 for 2 dpi or 3 dpi. Arrows denote cells that are positive for cleaved caspase 3. Black boxes show zoomed images. Scale bars are 100 μm (A, B, and D) and 1 mm (C).

Our previous work focused on E11 infection of the liver in hFcRn^{Tg32}-IFNAR$^{-/-}$ adult and neonatal mice (22). In the work presented here, we use a closely related virus, E5, to investigate the differential roles of type I and type III IFNs in CNS infection. While E11 and E5 both use human FcRn as their primary receptor, E11 also binds DAF (CD55) as an attachment factor, whereas E5 infection occurs independent of DAF binding (10). Previous studies showed that humanized DAF-expressing mice are not susceptible to a DAF-binding isolate of CVB by the enteral route (36), suggesting that DAF binding likely does not play a role in CVB infection *in vivo*. However, given that much less is known regarding the role of human or murine DAF in echovirus pathogenesis, we focused our current work on E5, which does not bind DAF and thus allowed us to define the specific role of FcRn in echovirus infections in the brain.

FcRn is expressed on the microvasculature of the BBB (16), where it has been proposed to mediate the efflux of antibodies out of the brain (37). In addition to this localization, FcRn is expressed in the epithelium of the choroid plexus (16). This pattern of expression is conserved between humans and hFcRn^{Tg32} mice (38). In addition to these sites, our data show that FcRn is expressed in distinct regions of the meninges. The meninges are composed of diverse cell types, with distinct patterns of expression regionally in the dura, arachnoid layer, and pia mater; the arachnoid layer and pia mater are referred to as the leptomeninges (39). The meningeal layers are primarily composed of fibroblasts, with each subtype expressing its own unique transcriptional signature (39). In addition to fibroblasts, the arachnoid layer contains arachnoid barrier cells, which are epithelium-like in origin and separate the dura mater from the subarachnoid space, in which CSF accesses the brain. The meninges also contain a large population of immune cells, including CD4$^+$ T cells and B cells. Notably, meningeal macrophages are a specialized subclass of macrophages that are long lived in the leptomeninges (40). We observed the highest levels of E5 infection restricted to the leptomeninges (the inner layer of the meninges containing the pia mater and arachnoid layer), which also expressed high levels of FcRn. Given the robust levels of E5 infection in the meninges, it is likely that fibroblasts are at least one target of infection. However, it is possible that other cell types, such as macrophages, are also permissive to infection and contribute to pathogenesis. Collectively, these data suggest that the regional expression of FcRn plays a direct role in the tropism of echoviruses in the brain and directly correlates with their high levels of replication in the meninges.

Several studies have investigated the levels of cytokines and chemokines within the CSF of infants and children with confirmed echovirus-induced meningitis. The CSF of children with E30-induced meningitis contains very high levels of MCP-1 and IL-6, compared to controls (24, 41). While we cannot sample CSF from a neonatal animal, our data show that hFcRn^{Tg32}-IFNAR$^{-/-}$ animals also induce very high levels of MCP-1 and IL-6 in brain tissue homogenates, which may contain some CSF. MCP-1, also known as CCL2, is a monocyte chemoattractant responsible for recruiting monocytes and dendritic cells to the site of inflammation due to infection. IL-6 is a proinflammatory cytokine that is secreted by macrophages that have detected a viral infection. These immune mediators play important roles in alerting the immune system to a viral infection and recruiting immune cells to the sites of infection. Given that induction of both MCP-1 and IL-6 is mediated through NF-κB-mediated signaling, they can be induced independent of any type I IFN-mediated signaling. However, because we used brain tissue homogenates and human studies can are restricted to CSF, it is unclear which cytokines induced by echovirus infections mediate the influx of immune cells observed in echovirus-induced meningitis in humans. Although the different roles of type I and type III IFNs in the respiratory and intestinal epithelium during enterovirus infection have been established (32, 42–44), whether these IFNs play distinct roles in enterovirus-induced meningitis has remained unclear. Our data suggest that type I IFNs are the sole barrier to disseminated echovirus infection that causes CNS disease, which is consistent with previous work indicating that these IFNs form at least one bottleneck to poliovirus access to the CNS (45). However, type I IFNs were not detected in multiplex

Luminex profiling of brain homogenates from echovirus-infected mice, suggesting that these IFNs are not produced locally in the brain. Therefore, it is likely that circulating IFNs produced in distal sites, such as the liver, trigger antiviral responses in the CNS that protect from echovirus infections.

In humans, neonates are at increased risks for echovirus-induced morbidity and death. For example, rates of echovirus-induced paralysis decreased with increased age at inoculation (46). Our previous work showed that adult echovirus-infected mice exhibit low levels of infection in the brain following i.p. inoculation (22). Our data presented here show that neonatal mice are highly sensitive to echovirus-induced neuronal dysfunction and contain high levels of viral infection within the meninges. The mechanistic basis for age-related differences in echovirus infection of the brain remains unclear. Given that the BBB forms in mice prior to birth (47), this barrier is unlikely to participate in these age-related differences. Age-related differences in neuronal susceptibility to infections are not specific to echoviruses and have also been shown for reovirus (48). However, unlike that work, our data suggest that type I IFNs are not the primary drivers for differential age susceptibility, given that both adult and neonatal animals in our work were deficient in IFNAR expression. Other work has shown that age-related differences in susceptibility to cardiac infections by CVB may result from differences in receptor expression (49, 50). Age-related differences in FcRn expression in humans are unknown, but its expression in human liver is not dependent on age (51), suggesting that this is unlikely to explain age-related differences in echovirus-associated neuronal infections. Therefore, it remains unclear which factors contribute to age-related differences in infection of the CNS.

Our findings presented here define key aspects of echovirus infection of the brain, including the sites of viral replication and the consequences of this infection. We show that FcRn is necessary but not sufficient for echovirus infection of the brain *in vivo* and that type I IFNs control infection within the meninges. Collectively, these studies develop a model of echovirus aseptic meningitis, which could aid in the testing of novel therapeutics.

MATERIALS AND METHODS

Cell lines and viruses. HeLa cells (clone 7B) were provided by Jeffrey Bergelson, Children's Hospital of Philadelphia (Philadelphia, PA), and cultured in minimal essential medium (MEM) supplemented with 5% fetal bovine serum (FBS), nonessential amino acids, and penicillin-streptomycin. Experiments were performed with E5 (Noyce strain), which was obtained from the ATCC. Virus was propagated in HeLa 7B cells and purified by ultracentrifugation over a 30% sucrose cushion, as described previously (52). The purity of viral stocks was confirmed by Sanger sequencing of VP1 using enterovirus-specific primers (32, 53).

Animals. All animal experiments were approved by the Duke University Animal Care and Use Committees, and all methods were performed in accordance with the relevant guidelines and regulations. C57BL/6J (WT [catalog no. 000664]), B6.Cg-*Fcgr*^{tm1Dcr}Tg(FCGRT)32Dcr/DcrJ (hFcRn^{Tg32} [catalog no. 014565]), and B6.(Cg)-Ifnar1$^{tm1.2Ees}$/J (IFNAR$^{-/-}$ [catalog no. 028288]) mice were purchased from the Jackson Laboratory. hFcRn^{Tg32}-IFNAR$^{-/-}$ mice were generated as described previously and were provided by Sujan Shresta (22). B6.Ifnlr$^{-/-}$/J (IFNLR$^{-/-}$) mice were provided by Megan Baldridge. hFcRn^{Tg32}-IFNLR$^{-/-}$ mice were generated as described (32). All animals used in this study were genotyped by Transnetyx, and genotyping assay results are available upon request.

Suckling pup infections. Seven-day-old mice were inoculated by the i.p. route with 10^4 or 10^3 PFU of E5. Inoculation was performed using a 1-mL disposable syringe and a 27-gauge needle, with 50 μL of 1$\times$ phosphate-buffered saline (PBS) and virus. A wellness/survival check was performed every 12 h over the course of infection; animals were monitored for clinical disease symptoms at these times. Pups were monitored for delayed movement in returning to their littermates when moved outside the litter, hindlimb weakness based on the ability to use the limbs while walking and potential dragging of limbs when set on a flat surface, severe delayed motor skills if animals had trouble walking back to their littermates or on a flat surface, or moribundity/death, which were all recorded. Mice were euthanized at either 1, 2, or 3 dpi, and organs were harvested into 0.5 mL of Dulbecco's modified Eagle's medium (DMEM) and stored at −80°C. Tissue samples for viral titration were thawed and homogenized with a TissueLyser LT (Qiagen) for 5 min, followed by brief centrifugation for 5 min at 8,000 $\times$ *g*. Viral titers in organ homogenates were determined by 50% tissue culture infective dose ($TCID_{50}$) assays in HeLa cells and enumerated following crystal violet staining.

Luminex assays. Luminex profiling was performed on whole-brain tissue homogenates that had been stored in 0.5 mL of DMEM at −80°C until use. Tissues were homogenized with a TissueLyser LT (Qiagen) for 5 min, followed by centrifugation at 10,000 $\times$ *g* for 10 min. Luminex kits that were used were a custom mouse IFN kit (IFN-α, IFNβ, and IL-28; Invitrogen), a mouse cytokine 23-plex (M60009RDPD; Bio-Rad), and a

TABLE 1 E5 HCR probes

Probe pair name	Odd	Even
B4P1	CCTCAACCTACCTCCAACAAGGGCTCAGTAAACTTTCCCGGGTCT	CATGGATTTGATCATAAGGTCCTTCATTCTCACCATATTCGCTTC
B4P2	CCTCAACCTACCTCCAACAAAGCCCTGATGGAACTTAGATGCGTT	CTTCAGGCACACACACCACCAGGAGATTCTCACCATATTCGCTTC
B4P3	CCTCAACCTACCTCCAACAAGCATTACTATGGTGGCACAATTGTT	TGTCCATCGGTACGCTATTAATGTAATTCTCACCATATTCGCTTC
B4P4	CCTCAACCTACCTCCAACAATGCTGCACCATCCTATAGTGGGTTT	ATGTAGCCTGCTGCTGAGTATTCATATTCTCACCATATTCGCTTC
B4P5	CCTCAACCTACCTCCAACAAGTTATGCTCAGACTTGGGCACGTCA	TTGGCCAAAGGCTCCATATGTGTGCATTCTCACCATATTCGCTTC
B4P6	CCTCAACCTACCTCCAACAAGTGATCAGGTCATCGTGATTTCTTA	CCAATGAGGGCTAGTGTGGCAGTCAATTCTCACCATATTCGCTTC
B4P7	CCTCAACCTACCTCCAACAAGATCTTCCAATTAGATTTGTTGCTA	ACTGAGCTGTTAAGCTTTTCAGCTAATTCTCACCATATTCGCTTC
B4P8	CCTCAACCTACCTCCAACAACTCCCTGTATAACGGTGGTCCCTGA	TGTCTCTGGTGCAACACTAATTTTGATTCTCACCATATTCGCTTC
B4P9	CCTCAACCTACCTCCAACAATTAGTGGGCGTGCCGCCCAGGTTTA	GTGGGGAAGTTATACATGAGCATTCATTCTCACCATATTCGCTTC
B4P10	CCTCAACCTACCTCCAACAAAGCGCTTCAAGACCCTCAGTACCGT	TGGGTAACCGGCGCTCGTTGTTAGATATTCTCACCATATTCGCTTC
B4P11	CCTCAACCTACCTCCAACAATGCACAAGTAGTCAATGTAGTTAGT	GCTTGTCTCTGTACAGGTGATGGGAATTCTCACCATATTCGCTTC
B4P12	CCTCAACCTACCTCCAACAATTTCACGAATGTTGATCTCCCACCT	TCTCACACTTTCTACGTAGTTGCACATTCTCACCATATTCGCTTC

mouse CXCL10 singleplex (EPX01A-26018-901; Invitrogen), according to the manufacturer's protocol. Assays were read on a BioPlex 200 system (Bio-Rad). Heatmaps were generated using the fold changes in concentration (picograms per milliliter) for each animal, compared to the average for uninfected animals, and were made with GraphPad Prism. Violin plots are shown as the concentration for each animal (one point) in picograms per milliliter.

Immunohistochemistry. Tissues were fixed in 10% buffered formalin for 24 h and then transferred to 70% ethanol. Tissues were embedded in paraffin and sectioned at the Duke Research Immunohistopathology core. Slides were stained with cleaved caspase 3 (Asp175) (9661; Cell Signaling) or human Fc gamma receptor and transporter (FCGRT) (ab139152; Abcam). Tissue sections were deparaffinized with xylene, rehydrated with decreasing concentrations of ethanol (100%, 95%, and 80%), and then washed with double-distilled H_2O. Antigen unmasking was performed with slides submerged in 10 mM citrate buffer (pH 6.0) and heated in a steamer for 20 min at ~90°C. Slides were allowed to cool to room temperature and were immunostained with cleaved caspase 3 or FCGRT using the Vectastain Elite ABC-horseradish peroxidase (HRP) kit (PK-6100; Vector Biolabs), according to the manufacturer's instructions. Slides were incubated in 6% H_2O_2 in methanol for 30 min and then washed three times for 5 min in H_2O. Avidin block (SP-2001; Vector) was applied for 15 min and washed twice in H_2O, followed by biotin block (ab156024; Abcam) for 15 min and washing twice in H_2O. Finally, serum-free protein block was applied for 10 min, cleaved caspase 3 antibody was diluted 1:100 and the FCGRT antibody 1:200 in Tris-buffered saline with 0.1% Tween 20 (TBS-T), and slides were incubated overnight at 4°C in a humidified chamber. Next, slides were washed three times for 5 min in 0.1% PBS-Tween (PBST) and exposed to the goat anti-rabbit IgG biotinylated secondary antibody (BA-1000; Vector) for 30 min. Slides were rinsed in PBST three times for 5 min, and the Vectastain Elite ABC-HRP kit was applied for 30 min. Slides were rinsed in PBST three times for 5 min and incubated with diaminobenzidine substrate for 5 min; the incubation was terminated with water incubation. Slides were counterstained with hematoxylin for 1 min, thoroughly rinsed with H_2O, and incubated in 0.1% sodium bicarbonate in H_2O for 5 min. Slides were then dehydrated with increasing concentrations of ethanol, cleared with xylene, and mounted with Cytoseal 60 (83104; Thermo Fisher Scientific). Images were captured on an IX83 inverted microscope (Olympus) using a UC90 color charge-coupled device (CCD) camera (Olympus).

HCR and imaging. HCR was performed following the Molecular Instruments HCR v3.0 protocol for formalin-fixed paraffin-embedded human tissue sections (34, 35). Briefly, tissue sections were deparaffinized with xylene and rehydrated with decreasing concentrations of ethanol (100%, 95%, and 80%). Antigen unmasking was performed with slides submerged in 10 mM citrate buffer (pH 6.0) and heated in a steamer for 20 min at ~90°C. Slides were cooled to room temperature, treated with 10 μg/mL proteinase K for 10 min at 37°C, and washed with RNase-free water. Samples were incubated for 10 min at 37°C in hybridization buffer. Sections were incubated overnight at 37°C in a humidified chamber with 3 pmol of initiator probes in prewarmed hybridization buffer. We designed probes for E5 in-house (Table 1). The next day, slides were washed in probe wash buffer and 5× SSCT (5 × SSC with 0.1% Tween 20; 1× SSC is 0.15 M NaCl plus 0.015 M sodium citrate) four times for 15 min, according to the manufacturer's instructions. Samples were incubated in a humidified chamber at 37°C for 30 min in amplification buffer. Fluorescent hairpins were heated to 95°C for 90 s and snap cooled at room temperature for 30 min. Hairpins and amplification buffer were added to the sample and incubated overnight at room temperature. Hairpins were washed off with 5× SSCT for 5 min, 15 min, 15 min, and 5 min, followed by a wash with PBS containing 4′,6-diamidino-2-phenylindole (DAPI). Slides were mounted in Vectashield with DAPI. Slides were imaged on a Zeiss 880 inverted confocal microscope with Airyscan. Image analysis was performed using Fiji.

Statistics. All statistical analyses were performed using GraphPad Prism version 9. Data are presented as mean ± standard deviation. Parametric tests were applied when data were distributed normally based on D'Agostino-Pearson analyses; otherwise, nonparametric tests were applied. The log rank test was used to analyze the statistical differences of the survival rates in Kaplan-Meier curves. In most cases, a Kruskal-Wallis test with a Dunn's test for multiple comparisons or two-way analysis of variance

(ANOVA) with Šídák's multiple-comparison test was used to determine statistical significance, as described in the figure legends. *P* values of <0.05 were considered statistically significant.

ACKNOWLEDGMENTS

We thank Cristian Ovies and Kalena Grimes (Duke University School of Medicine) for technical assistance, Megan Baldridge (Washington University) for providing IFNLR$^{-/-}$ mice, and Sujan Shresta (La Jolla Institute for Immunology) for providing hFcRn^{Tg32}-IFNAR$^{-/-}$ mice.

This project was supported by NIH grants R01-AI150151 (C.B.C.), T32-AI060525 (A.I.W.), and F31-AI149866 (A.I.W.).

The funders had no role in study design, data collection and analysis, the decision to publish, or preparation of the manuscript.

REFERENCES

1. Berlin LE, Rorabaugh ML, Heldrich F, Roberts K, Doran T, Modlin JF. 1993. Aseptic meningitis in infants <2 years of age: diagnosis and etiology. J Infect Dis 168:888–892. https://doi.org/10.1093/infdis/168.4.888.
2. Huang C, Morse D, Slater B, Anand M, Tobin E, Smith P, Dupuis M, Hull R, Ferrera R, Rosen B, Grady L. 2004. Multiple-year experience in the diagnosis of viral central nervous system infections with a panel of polymerase chain reaction assays for detection of 11 viruses. Clin Infect Dis 39:630–635. https://doi.org/10.1086/422650.
3. Rotbart HA. 1995. Enteroviral infections of the central nervous system. Clin Infect Dis 20:971–981. https://doi.org/10.1093/clinids/20.4.971.
4. Centers for Disease Control and Prevention. 2003. Outbreaks of aseptic meningitis associated with echoviruses 9 and 30 and preliminary surveillance reports on enterovirus activity–United States, 2003. MMWR Morb Mortal Wkly Rep 52:761–764.
5. Lee H-Y, Chen C-J, Huang Y-C, Li W-C, Chiu C-H, Huang C-G, Tsao K-C, Wu C-T, Lin T-Y. 2010. Clinical features of echovirus 6 and 9 infections in children. J Clin Virol 49:175–179. https://doi.org/10.1016/j.jcv.2010.07.010.
6. Kim H-J, Kang B, Hwang S, Hong J, Kim K, Cheon D-S. 2012. Epidemics of viral meningitis caused by echovirus 6 and 30 in Korea in 2008. Virol J 9:38. https://doi.org/10.1186/1743-422X-9-38.
7. Chuang YY, Huang YC. 2019. Enteroviral infection in neonates. J Microbiol Immunol Infect 52:851–857. https://doi.org/10.1016/j.jmii.2019.08.018.
8. Modlin JF. 1986. Perinatal echovirus infection: insights from a literature review of 61 cases of serious infection and 16 outbreaks in nurseries. Rev Infect Dis 8:918–926. https://doi.org/10.1093/clinids/8.6.918.
9. Centers for Disease Control and Prevention. 2006. Enterovirus surveillance–United States, 2002–2004. MMWR Morb Mortal Wkly Rep 55:153–156.
10. Morosky S, Wells AI, Lemon K, Evans AS, Schamus S, Bakkenist CJ, Coyne CB. 2019. The neonatal Fc receptor is a pan-echovirus receptor. Proc Natl Acad Sci U S A 116:3758–3763. https://doi.org/10.1073/pnas.1817341116.
11. Zhao X, Zhang G, Liu S, Chen X, Peng R, Dai L, Qu X, Li S, Song H, Gao Z, Yuan P, Liu Z, Li C, Shang Z, Li Y, Zhang M, Qi J, Wang H, Du N, Wu Y, Bi Y, Gao S, Shi Y, Yan J, Zhang Y, Xie Z, Wei W, Gao GF. 2019. Human neonatal Fc receptor is the cellular uncoating receptor for enterovirus B. Cell 177:1553–1565.e1516. https://doi.org/10.1016/j.cell.2019.04.035.
12. Pyzik M, Rath T, Lencer WI, Baker K, Blumberg RS. 2015. FcRn: the architect behind the immune and nonimmune functions of IgG and albumin. J Immunol 194:4595–4603. https://doi.org/10.4049/jimmunol.1403014.
13. Pyzik M, Rath T, Kuo TT, Win S, Baker K, Hubbard JJ, Grenha R, Gandhi A, Krämer TD, Mezo AR, Taylor ZS, McDonnell K, Nienaber V, Andersen JT, Mizoguchi A, Blumberg L, Purohit S, Jones SD, Christianson G, Lencer WI, Sandlie I, Kaplowitz N, Roopenian DC, Blumberg RS. 2017. Hepatic FcRn regulates albumin homeostasis and susceptibility to liver injury. Proc Natl Acad Sci U S A 114:E2862–E2871.
14. Chaudhury C, Mehnaz S, Robinson JM, Hayton WL, Pearl DK, Roopenian DC, Anderson CL. 2003. The major histocompatibility complex-related Fc receptor for IgG (FcRn) binds albumin and prolongs its lifespan. J Exp Med 197:315–322. https://doi.org/10.1084/jem.20021829.
15. Zhang Y, Pardridge WM. 2001. Mediated efflux of IgG molecules from brain to blood across the blood-brain barrier. J Neuroimmunol 114:168–172. https://doi.org/10.1016/S0165-5728(01)00242-9.
16. Schlachetzki F, Zhu C, Pardridge WM. 2002. Expression of the neonatal Fc receptor (FcRn) at the blood-brain barrier. J Neurochem 81:203–206. https://doi.org/10.1046/j.1471-4159.2002.00840.x.
17. Ahn J, Choi J, Joo CH, Seo I, Kim D, Yoon SY, Kim YK, Lee H. 2004. Susceptibility of mouse primary cortical neuronal cells to coxsackievirus B. J Gen Virol 85:1555–1564. https://doi.org/10.1099/vir.0.19695-0.
18. Feuer R, Pagarigan RR, Harkins S, Liu F, Hunziker IP, Whitton JL. 2005. Coxsackievirus targets proliferating neuronal progenitor cells in the neonatal CNS. J Neurosci 25:2434–2444. https://doi.org/10.1523/JNEUROSCI.4517-04.2005.
19. Feuer R, Mena I, Pagarigan RR, Harkins S, Hassett DE, Whitton JL. 2003. Coxsackievirus B3 and the neonatal CNS: the roles of stem cells, developing neurons, and apoptosis in infection, viral dissemination, and disease. Am J Pathol 163:1379–1393. https://doi.org/10.1016/S0002-9440(10)63496-7.
20. Hughes SA, Thaker HM, Racaniello VR. 2003. Transgenic mouse model for echovirus myocarditis and paralysis. Proc Natl Acad Sci U S A 100:15906–15911. https://doi.org/10.1073/pnas.2535934100.
21. Zhang G, Li J, Sun Q, Zhang K, Xu W, Zhang Y, Wu G. 2021. Pathological features of echovirus-11-associated brain damage in mice based on RNA-Seq analysis. Viruses 13:2477. https://doi.org/10.3390/v13122477.
22. Wells AI, Grimes KA, Kim K, Branche E, Bakkenist CJ, DePas WH, Shresta S, Coyne CB. 2021. Human FcRn expression and type I interferon signaling control echovirus 11 pathogenesis in mice. PLoS Pathog 17:e1009252. https://doi.org/10.1371/journal.ppat.1009252.
23. Nishikawa M, Matsubara T, Yoshitomi T, Ichiyama T, Hayashi T, Furukawa S. 2000. Abnormalities of brain perfusion in echovirus type 30 meningitis. J Neurol Sci 179:122–126. https://doi.org/10.1016/S0022-510X(00)00398-1.
24. Wang S-M, Lei H-Y, Su L-Y, Wu J-M, Yu C-K, Wang J-R, Liu C-C. 2007. Cerebrospinal fluid cytokines in enterovirus 71 brain stem encephalitis and echovirus meningitis infections of varying severity. Clin Microbiol Infect 13:677–682. https://doi.org/10.1111/j.1469-0691.2007.01729.x.
25. Ichiyama T, Maeba S, Suenaga N, Saito K, Matsubara T, Furukawa S. 2005. Analysis of cytokine levels in cerebrospinal fluid in mumps meningitis: comparison with echovirus type 30 meningitis. Cytokine 30:243–247. https://doi.org/10.1016/j.cyto.2005.01.022.
26. Chonmaitree T, Baron S. 1991. Bacteria and viruses induce production of interferon in the cerebrospinal fluid of children with acute meningitis: a study of 57 cases and review. Rev Infect Dis 13:1061–1065. https://doi.org/10.1093/clinids/13.6.1061.
27. Singh H, Koury J, Kaul M. 2021. Innate immune sensing of viruses and its consequences for the central nervous system. Viruses 13:170. https://doi.org/10.3390/v13020170.
28. Lazear HM, Daniels BP, Pinto AK, Huang AC, Vick SC, Doyle SE, Gale M, Jr., Klein RS, Diamond MS. 2015. Interferon-λ restricts West Nile virus neuroinvasion by tightening the blood-brain barrier. Sci Transl Med 7:284ra259. https://doi.org/10.1126/scitranslmed.aaa4304.
29. Li Y, Zhao L, Luo Z, Zhang Y, Lv L, Zhao J, Sui B, Huang F, Cui M, Fu ZF, Zhou M. 2020. Interferon-λ attenuates rabies virus infection by inducing interferon-stimulated genes and alleviating neurological inflammation. Viruses 12:405. https://doi.org/10.3390/v12040405.
30. Wells AI, Coyne CB. 2018. Type III interferons in antiviral defenses at barrier surfaces. Trends Immunol 39:848–858. https://doi.org/10.1016/j.it.2018.08.008.
31. Roopenian DC, Christianson GJ, Proetzel G, Sproule TJ. 2016. Human FcRn transgenic mice for pharmacokinetic evaluation of therapeutic antibodies. Methods Mol Biol 1438:103–114. https://doi.org/10.1007/978-1-4939-3661-8_6.

32. Wells AI, Grimes KA, Coyne CB. 2022. Enterovirus replication and dissemination are differentially controlled by type I and III interferons in the gastrointestinal tract. mBio 13:e00443-22. https://doi.org/10.1128/mbio.00443-22.
33. Bergelson JM, Chan M, Solomon KR, St John NF, Lin H, Finberg RW. 1994. Decay-accelerating factor (CD55), a glycosylphosphatidylinositol-anchored complement regulatory protein, is a receptor for several echoviruses. Proc Natl Acad Sci U S A 91:6245–6248. https://doi.org/10.1073/pnas.91.13.6245.
34. Choi HMT, Schwarzkopf M, Fornace ME, Acharya A, Artavanis G, Stegmaier J, Cunha A, Pierce NA. 2018. Third-generation in situ hybridization chain reaction: multiplexed, quantitative, sensitive, versatile, robust. Development 145:dev165753. https://doi.org/10.1242/dev.165753.
35. Choi HMT, Calvert CR, Husain N, Huss D, Barsi JC, Deverman BE, Hunter RC, Kato M, Lee SM, Abelin ACT, Rosenthal AZ, Akbari OS, Li Y, Hay BA, Sternberg PW, Patterson PH, Davidson EH, Mazmanian SK, Prober DA, van de Rijn M, Leadbetter JR, Newman DK, Readhead C, Bronner ME, Wold B, Lansford R, Sauka-Spengler T, Fraser SE, Pierce NA. 2016. Mapping a multiplexed zoo of mRNA expression. Development 143:3632–3637. https://doi.org/10.1242/dev.140137.
36. Pan J, Zhang L, Odenwald MA, Shen L, Turner JR, Bergelson JM. 2015. Expression of human decay-accelerating factor on intestinal epithelium of transgenic mice does not facilitate infection by the enteral route. J Virol 89:4311–4318. https://doi.org/10.1128/JVI.03468-14.
37. Cooper PR, Ciambrone GJ, Kliwinski CM, Maze E, Johnson L, Li Q, Feng Y, Hornby PJ. 2013. Efflux of monoclonal antibodies from rat brain by neonatal Fc receptor, FcRn. Brain Res 1534:13–21. https://doi.org/10.1016/j.brainres.2013.08.035.
38. Latvala S, Jacobsen B, Otteneder MB, Herrmann A, Kronenberg S. 2017. Distribution of FcRn across species and tissues. J Histochem Cytochem 65:321–333. https://doi.org/10.1369/0022155417705095.
39. DeSisto J, O'Rourke R, Jones HE, Pawlikowski B, Malek AD, Bonney S, Guimiot F, Jones KL, Siegenthaler JA. 2020. Single-cell transcriptomic analyses of the developing meninges reveal meningeal fibroblast diversity and function. Dev Cell 54:43–59.e44. https://doi.org/10.1016/j.devcel.2020.06.009.
40. Kierdorf K, Masuda T, Jordao MJC, Prinz M. 2019. Macrophages at CNS interfaces: ontogeny and function in health and disease. Nat Rev Neurosci 20:547–562. https://doi.org/10.1038/s41583-019-0201-x.
41. Matsubara T, Matsuoka T, Katayama K, Yoshitomi T, Nishikawa M, Ichiyama T, Furukawa S. 2000. Mononuclear cells and cytokines in the cerebrospinal fluid of echovirus 30 meningitis patients. Scand J Infect Dis 32:471–474.
42. Drummond CG, Bolock AM, Ma C, Luke CJ, Good M, Coyne CB. 2017. Enteroviruses infect human enteroids and induce antiviral signaling in a cell lineage-specific manner. Proc Natl Acad Sci U S A 114:1672–1677. https://doi.org/10.1073/pnas.1617363114.
43. Freeman MC, Wells AI, Ciomperlik-Patton J, Myerburg MM, Yang L, Konopka-Anstadt J, Coyne CB. 2021. Respiratory and intestinal epithelial cells exhibit differential susceptibility and innate immune responses to contemporary EV-D68 isolates. Elife 10:e66687. https://doi.org/10.7554/eLife.66687.
44. Good C, Wells AI, Coyne CB. 2019. Type III interferon signaling restricts enterovirus 71 infection of goblet cells. Sci Adv 5:eaau4255. https://doi.org/10.1126/sciadv.aau4255.
45. Kuss SK, Etheredge CA, Pfeiffer JK. 2008. Multiple host barriers restrict poliovirus trafficking in mice. PLoS Pathog 4:e1000082. https://doi.org/10.1371/journal.ppat.1000082.
46. Bultmann BD, Eggers HJ, Galle J, Haferkamp O. 1983. Age dependence of paralysis induced by echovirus type 9 in infant mice. J Infect Dis 147:999–1005. https://doi.org/10.1093/infdis/147.6.999.
47. O'Brown NM, Pfau SJ, Gu C. 2018. Bridging barriers: a comparative look at the blood-brain barrier across organisms. Genes Dev 32:466–478. https://doi.org/10.1101/gad.309823.117.
48. Wu AG, Pruijssers AJ, Brown JJ, Stencel-Baerenwald JE, Sutherland DM, Iskarpatyoti JA, Dermody TS. 2018. Age-dependent susceptibility to reovirus encephalitis in mice is influenced by maturation of the type-I interferon response. Pediatr Res 83:1057–1066. https://doi.org/10.1038/pr.2018.13.
49. Lyden D, Olszewski J, Huber S. 1987. Variation in susceptibility of Balb/c mice to coxsackievirus group B type 3-induced myocarditis with age. Cell Immunol 105:332–339. https://doi.org/10.1016/0008-8749(87)90081-5.
50. Khatib R, Chason JL, Silberberg BK, Lerner AM. 1980. Age-dependent pathogenicity of group B coxsackieviruses in Swiss-Webster mice: infectivity for myocardium and pancreas. J Infect Dis 141:394–403. https://doi.org/10.1093/infdis/141.3.394.
51. Qiu X, Wang MZ. 2020. Quantification of neonatal Fc receptor and beta-2 microglobulin in human liver tissues by ultraperformance liquid chromatography-multiple reaction monitoring-based targeted quantitative proteomics for applications in biotherapeutic physiologically-based pharmacokinetic models. Drug Metab Dispos 48:925–933. https://doi.org/10.1124/dmd.120.000075.
52. Morosky S, Lennemann NJ, Coyne CB. 2016. BPIFB6 regulates secretory pathway trafficking and enterovirus replication. J Virol 90:5098–5107. https://doi.org/10.1128/JVI.00170-16.
53. Oberste MS, Nix WA, Maher K, Pallansch MA. 2003. Improved molecular identification of enteroviruses by RT-PCR and amplicon sequencing. J Clin Virol 26:375–377. https://doi.org/10.1016/S1386-6532(03)00004-0.